NASA TECHNICAL MEMORANDUM 104197

NASA-TM-104197 19920009715

FATIGUE DAMAGE IN CROSS-PLY TITANIUM METAL MATRIX COMPOSITES CONTAINING CENTER HOLES

J. G. Bakuckas, Jr., W. S. Johnson
and C. A. Bigelow

January 1992

National Aeronautics and
Space Administration

LANGLEY RESEARCH CENTER
Hampton, Virginia 23665-5225

Abstract

The development of fatigue damage in $[0/90]_s$ SCS-6/Ti-15-3 laminates containing center holes was investigated. Stress levels required for crack initiation in the matrix were predicted using an effective strain parameter and compared to experimental results. Damage progression was monitored at various stages of fatigue loading. In general, a saturated state of damage consisting of matrix cracks and fiber-matrix debonding was obtained which reduced the composite modulus. Matrix cracks were bridged by the 0° fibers. The fatigue limit (stress causing catastrophic fracture of the laminates) was also determined. The static and post-fatigue residual strengths were accurately predicted using a three dimensional elastic-plastic finite element analysis. The matrix damage that occurred during fatigue loading significantly reduced the notched strength.

Nomenclature

E_L = Composite longitudinal modulus

E_T = Composite transverse modulus

G_{LT} = Composite shear modulus

K_t = Orthotropic stress concentration factor

K_t^{∞} = Orthotropic stress concentration factor for infinite sheet

R = Stress ratio

S_{max} = Maximum applied stress

S_{min} = Minimum applied stress

ΔS = Applied stress range

α = Isotropic finite width correction factor

$\Delta\varepsilon_{eff}$ = Modified effective strain parameter

$\Delta\varepsilon_{eff}^{ro}$ = Run-out value of effective strain parameter

ε_{max} = Maximum applied strain

$\Delta\varepsilon$ = Applied strain range

ν_{LT} = Composite Poisson's ratio

σ_m^r = Axial thermal residual stress in matrix

Introduction

Titanium metal matrix composites (MMC) have potential applications in the aerospace industry. The majority of these applications are for high strength, low weight structural components subjected to elevated temperatures. However, before MMC can be confidently used for such applications, the complex state of damage that develops in these materials must be addressed. The initiation and progression of damage in several MMC have been investigated [1-5]. It was found in these studies that damage in MMC consists primarily of fiber breakage, matrix cracking, matrix plastic deformation, and fiber-matrix debonding. The sequence and combination of these failure mechanisms depend on many variables including constituent properties, fabrication processes, applied loadings, specimen geometries, and heat treatments. A state of damage developed under certain circumstances may not cause catastrophic fracture of a component, but may affect the residual strength and life of the component.

The development of fatigue damage in titanium MMC having stress concentrations has been addressed in [2-5]. An analysis procedure for matrix crack initiation was introduced in [6] based on an effective strain parameter [7]. Using this analysis, the number of cycles to matrix crack initiation was accurately predicted in several lay-ups of SCS-6/Ti-15-3 containing center holes and double edge notches [6]. Observations of the damage growth behavior in similar SCS-6/Ti-15-3 specimen configurations revealed multiple matrix cracks which were bridged by the 0° fibers [5]. Matrix cracks typically were uniformly spaced in the net section regions away from the stress concentration [3]. In addition, fiber-matrix debonding in the 0° plies was observed near the center hole of the specimens tested in [5]. Fiber-matrix debonding was also observed in 90° plies of unnotched cross-ply laminates during static loading at low applied stress levels (approximately 22% of the static unnotched strength) [8].

The effects of fatigue damage on strength has been investigated in [9-11]. In certain composites, damage developed during fatigue loading can be beneficial. The post-fatigue residual

strength of certain notched composites is often higher than the virgin static notched strength [9-10]. Composites exhibiting such behavior contain matrix materials with yield or ultimate strengths that are low compared to the strength of the reinforcing fiber. Matrix damage at the notch tip such as matrix plastic deformation, matrix splitting, and fiber-matrix debonding reduce the stress concentrations resulting in higher post-fatigue residual strengths. However, in composites containing higher strength matrix materials such as SCS-6/Ti-15-3, the titanium matrix carries a larger portion of the load. Consequently, matrix damage results in greater loads being transferred to the fibers. The load transfer to the fibers is more significant than any decrease in the stress concentration due to matrix damage. The post-fatigue residual strength is therefore lower than the static notched strength. Johnson [11] reported a post-fatigue residual strength approximately 42% less than the virgin static notched strength in $[0/90]_{2S}$ SCS-6/Ti-15-3 specimens containing center holes. In order to accurately predict residual strength and life, it is necessary to understand the state of fatigue damage in the subject material.

The objective of this research was to study damage initiation and progression during fatigue loading in $[0/90]_S$ SCS-6/Ti-15-3 laminates containing center holes and to determine the effects of fatigue damage on the static notched strength. Initially, specimens were subjected to the maximum stress level at which no damage took place. An effective strain parameter which includes stress concentrations and matrix residual stresses was used to predict this stress level and the number of cycles to damage initiation. Next, specimens were loaded to a stress level at which extensive matrix cracking took place without fiber breakage. Damage progression was monitored and recorded. In addition, modulus loss due to fatigue damage was measured in the far-field region between the center hole and grips. Fatigue loading was terminated after matrix cracking reached a saturated level. Finally, post-fatigue residual strength was measured to determine the effect of fatigue damage. Static notched and post-fatigue residual strengths were predicted using a three dimensional elastic-plastic finite element analysis.

Materials and Test Procedures

Materials and Specimens

The titanium MMC studied in this work is designated SCS-6/Ti-15-3. The matrix specification Ti-15-3 is a shortened designation for the Ti-15V-3Cr-3Al-3Sn alloy. The composite laminates were made by hot-pressing Ti-15-3 foils between unidirectional tapes of silicon-carbide fibers held in place with molybdenum wires. The manufacturer's designation for these fibers is SCS-6. The SCS-6 fibers have a diameter of 0.14 mm. The lay-up studied was $[0/90]_S$ with a fiber volume fraction v_f of 0.355. All laminates tested were in the as-received condition.

All specimens were cut using a diamond wheel saw into straight-sided coupons with the 0° fibers in the loading direction. Each specimen was 19.05-mm wide and 152.4-mm long containing a 6.35-mm diameter center hole drilled ultrasonically. The 4-ply laminate was 0.89 mm thick. The surface of each specimen was polished to obtain a flat and lustrous finish. Brass end tabs were bonded on all specimens using a cyanoacrylate adhesive.

Test Procedures

Static and fatigue tests were conducted using a closed-loop servo-hydraulic test machine. The static tests were conducted under load control at a rate of 22.24 N/s. One unnotched specimen and one center hole specimen were tested statically in order to measure the elastic longitudinal modulus as well as the notched and unnotched strengths.

In the fatigue tests, cyclic tensile stress was applied under load control having an R-ratio (S_{min}/S_{max}) of 0.1 and a frequency of 10 Hz. The loading history of each specimen subjected to fatigue loading is shown in Table 1. Damage initiation and progression under fatigue loading were monitored and recorded using a closed-circuit television system (CCTV) having magnification capabilities of X325, an optical microscope, and replicas (surface and edge). The occurrence of matrix cracking and fiber-matrix debonding was determined. Modulus loss due to fatigue damage

was measured in the far-field region above the center hole and below the upper grip using a 25.4 mm gage length extensometer. In one specimen, the outer layer of matrix material was removed through an acid etching procedure to reveal fiber breaks. The post-fatigue residual strength was measured under static loading.

Analytical Procedures

Matrix Crack Initiation Stress Prediction

Hillberry and Johnson [6] predicted the onset of matrix cracking in several SCS-6/Ti-15-3 composite lay-ups containing center holes and double edge notches based on a modified effective strain parameter. In their study, the effective strain parameter developed by Smith, Watson and Topper [7] was modified for a composite material to include the effects of stress concentrations and thermal residual stresses as shown below [6]:

$$\Delta\varepsilon_{eff} = \sqrt{(K_t\varepsilon_{max} + \frac{\sigma_m^r}{E_m}) K_t \frac{\Delta\varepsilon}{2}} \qquad (1)$$

where K_t, ε_{max}, σ_m^r, E_m, and $\Delta\varepsilon$ are the orthotropic stress concentration factor, the maximum applied strain, the axial matrix thermal residual stress, the matrix modulus, and the applied strain range, respectively. Equation (1) does not account for circular hole size effects, the multiaxial state of strain in the matrix near a stress concentration, or damage on the composite microstructural scale (e.g., matrix cracks initiating from debonded fiber-matrix interfaces).

The matrix thermal residual stress in the fiber direction, σ_m^r, resulting from the cooldown during the fabrication process was calculated to be 213 MPa using a concentric cylinder micromechanics model [12]. The constitutive properties [8] shown in Table 2 and a thermal cooldown of 555°C were used to determine σ_m^r. Assuming linear elastic behavior, the maximum

strain and the strain range are related to the maximum far-field stress, S_{max}, as follows:

$$\varepsilon_{max} = \frac{S_{max}}{E_L} \quad \text{and} \quad \Delta\varepsilon = \frac{\Delta S}{E_L} = \frac{(1\text{-}R)S_{max}}{E_L} \tag{2}$$

where E_L is the laminate longitudinal modulus and $R = \frac{S_{min}}{S_{max}}$ is the stress ratio. Laminate properties were calculated from the constituent properties using the AGLPLY program [13] which uses the vanishing-fiber-diameter material model [13]. The constituent properties and the calculated laminate properties are shown in Table 2. The orthotropic stress concentration factor K_t was calculated as described in the Appendix. For the center hole $[0/90]_s$ specimens used here, K_t = 3.72. From Equations (1) and (2), the maximum stress for a given $\Delta\varepsilon_{eff}$ can be written as:

$$S_{max} = -\frac{\sigma_m^r E_L}{2K_t E_m} + \frac{1}{2}\sqrt{\left\{\frac{\sigma_m^r E_L}{K_t E_m}\right\}^2 + \frac{8}{(1\text{-}R)}\left\{\frac{\Delta\varepsilon_{eff} E_L}{K_t}\right\}^2} \tag{3}$$

The effective strain parameter as a function of cycles to failure for the Ti-15-3 matrix material was determined in [6] and is shown in Figure 1. The solid line is a curve fit to the experimental data. For a notched composite with thermal residual stresses, the number of cycles to matrix crack initiation can be predicted by comparing the modified effective strain parameter (Equation (1)) with the solid line in Figure 1. To predict the maximum stress level at which no matrix cracking will occur, the run-out value of the effective strain parameter $\Delta\varepsilon_{eff}^{ro}$ is required; $\Delta\varepsilon_{eff}^{ro}$ was assumed to be 0.002.

Post -Fatigue Strength Predictions

The post-fatigue residual strength was predicted using a three dimensional finite element program, PAFAC [14]. The 0° fiber axial stress next to the hole was predicted for the undamaged

virgin and the post-fatigue damaged conditions as a function of applied load. The composite strength was assumed to be the applied load at which the axial stress in the 0° fiber next to the hole reached the fiber strength.

The PAFAC analysis is based on constituent properties and uses the vanishing-fiber-diameter model [13] to account for the elastic-plastic behavior of the matrix and elastic behavior of the fiber. The nonlinear stress-strain response of the Ti-15-3 matrix was modeled using a multi-linear curve [8]. PAFAC uses eight-noded hexahedral elements; each element represents a unidirectional composite material whose fibers are arbitrarily oriented in the structural coordinate system. Using this material model, the analysis calculates the fiber and the laminate stresses.

Figure 2 shows a plan view of the finite element mesh used to model the center hole specimens. Due to symmetry in geometry and loading, only one eighth of the specimen was modeled. The finite element mesh contained 540 elements and 950 nodes. Each ply of the $[0/90]_s$ laminate was modeled with one layer of elements. The smallest elements located next to the hole were sized to represent one fiber spacing. This fiber spacing was calculated using the fiber volume fraction (v_f = 0.355), the fiber diameter (d_f = 0.14 mm), and the ply thickness (t = 0.223 mm). Forces were applied to the nodes at the end of the mesh so that the end displaced uniformly.

Through-the-thickness matrix cracking was modeled in the PAFAC analysis by using a reduced matrix modulus in the material properties. The AGLPLY [13] program was used to calculate the reduction in matrix modulus that corresponded to the measured reduction in composite longitudinal modulus. In the analysis, the reduced matrix modulus was used for the post-fatigue condition and the the original constituent properties were used for the virgin condition. Previous studies on unnotched cross-ply SCS-6/Ti-15-3 laminates reveal that fiber-matrix debonding in the 90° plies occurs at relatively low load levels (approximately 22% of the static unnotched strength) [8]. To model this phenomena in the virgin condition, the material properties of the 90° plies were

modified to represent an isotropic material having a modulus equivalent to the transverse modulus of a unidirectional lamina with complete fiber-matrix debonding as described in detail in [15]. This approximation is valid since plastic deformation was very limited.

Results and Discussion

Both the notched and unnotched static strengths were measured, Table 2. The static notched strength was approximately 48% of the unnotched strength. Similarly, the static notched strength was approximately 53% of the unnotched strength in $[0/90]_{2S}$ laminates containing center holes [15].

Results indicate that fatigue damage initiated as fiber-matrix debonding in the 90° plies and as matrix cracks growing from the debonded surfaces. In addition, matrix cracking took place in the 0° plies. The 0° fibers were intact in the wake of these matrix cracks.

Matrix Crack Initiation

Table 3 lists the predicted and observed number of cycles to matrix crack initiation for several specimens. The effective strain parameter was calculated using Equation (1) and this value was then used in Figure 1 to predict the number of cycles to matrix crack initiation. The solid line in this figure is a curve fit to the experimental data of the matrix material. Experimentally, matrix crack initiation was assumed when the crack length reached 0.5 mm. As shown in Table 3, the predictions and observations are in good agreement, particularly at the highest applied stress. The largest discrepancy occurred in attempting to predict the stress level below which no matrix cracking initiated.

The predicted maximum applied stress at which no matrix cracks occurred was $S_{max} = 93$ MPa using $\Delta\varepsilon_{eff}^{ro} = 0.002$ and Equation (3) (specimen number 1, Table 1). However at this

stress level, matrix cracks initiated between 250,000 and 300,000 cycles. Another specimen was cycled at an applied stress level of S_{max} = 80 MPa (specimen number 2, Table 1). At this stress level, no damage had initiated after 300,000 cycles. Thus, the maximum applied stress at which no matrix cracking takes place is assumed to be between S_{max} = 80 MPa and S_{max} = 93 MPa (15% and 18% of the static notched strength, respectively).

Matrix Crack Progression

Development of Matrix Cracks Near Center Hole

Figure 3 shows schematics taken directly from the CCTV monitor of matrix crack development during the fatigue loading of a specimen at S_{max} = 200 MPa (specimen number 1, Table 1). During this test, matrix cracking initiated at S_{max} = 93 MPa from the edge of the center hole, Figure 3(a) (cracks 1 and 2). These matrix cracks may have initiated from the first intact 0° fiber as was observed in [3] for $[0/90]_{2s}$ SCS-6/Ti-15-3 specimens containing center holes. As these matrix cracks continued to grow, secondary cracks formed in regions away from the edge of the center hole, Figure 3(b) (cracks 4 and 7). In addition, matrix cracks (cracks 3, 5 and 6) developed in regions above and below the original matrix cracks (cracks 1 and 2). Matrix cracks continued to propagate and link-up until cracking reached a saturated state, Figure 3(c). Saturation was assumed when no additional matrix cracks initiated and when existing cracks no longer grew. As shown in the figure, the matrix cracks have a uniform spacing a short distance (approximately 1 mm) away from the center hole. The spacing of these matrix cracks is approximately 0.9 mm which agrees with the predicted spacing of 0.85 mm for $[0/90]_{2s}$ SCS-6/Ti-15-3 laminates containing center holes [3]. Similar cracking patterns (multiple matrix cracks) were observed in [5] for $[0/90]_{2s}$ SCS-6/Ti-15-3 laminates containing center holes.

The total crack length as a function of the number of cycles is shown in Figure 4 for three specimens subjected to different maximum stress levels. For each specimen, the length of all matrix cracks within the same area near the center hole was summed. As shown in the figure, the

total crack length approached a maximum value, which corresponded to matrix crack saturation, for each stress level. The number of cycles at which the matrix cracking reached a saturated state decreased as the applied stress increased. In addition, the total crack length was greater for higher stress levels. For S_{max} = 200 MPa and 250 MPa, the total matrix crack length approaches constant values of 43 mm and 48 mm, respectively. For S_{max} = 150 MPa, the matrix crack length appears to be still increasing at 250,000 cycles, indicating saturation was not reached.

Development of Matrix Cracks in Far-Field Region

Matrix cracks in the far-field region appeared to have a uniform crack pattern as shown schematically in Figure 5(a) for a specimen subjected to S_{max} = 265 MPa for 1,000,000 cycles. The region of uniform matrix cracks starts approximately 10.5 mm above and below the centerline of the hole. The figure also shows a photograph (Figure 5(b)) of the specimen edge in the region of uniform crack spacing. As shown, the uniform matrix cracks are through-the-thickness cracks and appear to have originated at the debonded 90° fiber-matrix interfaces. These through-the-thickness cracks were also observed on interior planes across the width of the specimen (not shown). It was shown in [8] that debonding of the 90° fiber-matrix interface occurs at a relatively low stress level (approximately 22% of the unnotched strength for $[0/90]_{2s}$ laminates). This debonded interface served as the initiation site for matrix cracking. These matrix cracks progressed to the 0° fibers, where debonding of the 0° fiber-matrix interface may have taken place, and eventually grew around to the outer surface. From Figure 5(b), the spacing of the uniform, through-the-thickness cracks is approximately 1 mm. The initiation of matrix cracks at the debonded 90° fiber-matrix interfaces was also observed in $[0/90]_{2s}$ SCS-6/Ti-15-3 laminates [3].

Reduction in Modulus

The composite loading modulus in the longitudinal direction for a specimen subjected to S_{max} = 250 MPa for 200,000 cycles was measured in the far-field region above the center hole and below the upper grip using a 25.4-mm gage length extensometer during fatigue loading.

Figure 6 shows the normalized composite longitudinal modulus measured during initial portion of the loading cycle as a function of the number of cycles. The modulus was normalized with respect to the initial modulus, E_L = 168.43 GPa. Also shown in this figure are edge replicas taken in the gage section of the extensometer illustrating the damage that took place through the specimen thickness at several fatigue cycle numbers. The modulus was reduced progressively with increasing loading cycles as a result of fatigue damage. After the first cycle, a reduction in the modulus of 10% was measured due to the initiation of failure of the 90° ply fiber-matrix interfaces. Fiber-matrix separation is seen in the edge replica taken after the first cycle as the dark line in the interface region. A 15% reduction in modulus was measured after 1000 cycles due to further debonding in the 90° ply fiber-matrix interfaces. During the next 24,000 cycles, no other damage was observed and the modulus decreased slightly. A greater rate of decrease in the modulus was noted after 24,000 cycles. This corresponds to the initiation of matrix cracks from the debonded 90° ply fiber-matrix interfaces as shown in the replica taken after 40,000 cycles. These matrix cracks apparently progress to the outer surface as shown in the replica taken after 120,000 cycles. The modulus continued to reduce slightly and approached an asymptotic value corresponding to matrix crack saturation which occurred at approximately 120,000 cycles. A reduction of 38% in the composite modulus was measured after 200,000 cycles.

Fatigue Limit

The maximum stress level at which a specimen can be fatigued without causing catastrophic fracture (i.e. the fatigue limit) was determined experimentally. The 0° fibers must fail prior to catastrophic fracture. An incremental load approach was used for two specimens (specimens number 1 and 2) as shown in Table 1. The applied stress level was increased after fatigue damage reached a saturated state. This incrementally increasing load history was applied until the specimen fractured. In specimen numbers 1 and 2, fracture occurred at S_{max} = 308 MPa after 1710 cycles, and at S_{max} = 265 MPa after 56,169 cycles, respectively. As shown in Table 1, another specimen (specimen number 3) was fatigued for 1,000,000 cycles at a stress level of S_{max} = 265

MPa. Figure 7 shows two photographs of this specimen after fatigue cycling. Figure 7(a) shows a surface replica indicating the extensive matrix cracking that took place. Figure 7(b) shows the same region with the outer layer of matrix material removed by an acid etching technique. In this photograph, only the first fiber next to the hole is fractured (possibly damaged during drilling of the center hole). The stress level was lowered to S_{max} = 250 MPa for another specimen (specimen number 4) and that specimen was fatigued for 200,000 cycles without fiber failure. Based on these results, it was assumed that fiber failure will not occur at a stress level below S_{max} = 265 MPa. This stress level is approximately 50% of the static notched strength (525 MPa).

Post -Fatigue Residual Strength

The post-fatigue residual strength was determined from a specimen that had been subjected to S_{max} = 250 MPa for 200,000 cycles during which matrix cracking reached a saturated level, (specimen number 4, Table 1). The specimen was loaded quasi-statically in tension to failure and a residual strength of 325 MPa was measured. This value is a 38% reduction in strength compared to that in the virgin specimen (525 MPa). Johnson [11] reported a 42% reduction in strength due to fatigue damage in a $[0/90]_{2s}$ laminate containing a center hole (v_f = 0.325).

A three dimensional finite element analysis (PAFAC) was used to determine the effects of matrix cracking on the 0° fiber stress concentration and to predict the residual strength of both the virgin and post-fatigued specimens. The 0° axial fiber stress in the element next to the center hole was calculated for the virgin and post-fatigue conditions. For the virgin condition, the constituent properties shown in Table 2 were used. In addition, fiber-matrix debonding in the 90° plies was modeled as described in [15]. For the post-fatigue condition, matrix cracking was accounted for using a reduced matrix modulus. As described earlier, extensive matrix cracking was observed as shown schematically in Figure 8(a). From this figure, a small region located directly above and below the center hole developed no matrix cracks. To account for this matrix crack pattern, the properties of the elements in the 0° and 90° plies were modified as shown in Figure 8(b). In

regions where no matrix cracking occurred, elements retained their original properties (shaded area in Figure 8(b)). In regions of matrix cracking, the matrix modulus was reduced by 69%. The 69% reduction in matrix modulus was determined using AGLPLY [13] and corresponds to the measured 38% reduction in the composite longitudinal modulus, Figure 6.

Figure 9 shows the axial stress in the 0° fiber next to the center hole as a function of the applied stress. The horizontal line indicates the assumed fiber strength of 4400 MPa, and the two vertical lines show the experimental strengths of the two conditions. The fiber strength was calculated from the measured strain to failure of an $[0/90]_s$ unnotched specimen ($\varepsilon_f^{ult} = 0.0011$) multiplied by the fiber modulus (400 GPa). As shown in Figure 9, the applied stress at which the 0° fiber stress equals the fiber strength corresponds closely to the measured strength for both conditions. Using the axial stress in the 0° fiber next to the center hole as the criterion for laminate failure, the predicted strengths for the virgin and post-fatigue conditions were 483 MPa and 301 MPa, respectively. Both predictions are within 8% of the experimental values.

The decrease in residual strength due to matrix cracking is significant. The fact that these matrix cracks initiated and grew under cyclic stress levels that were approximately 18% of the static notched strength is disturbing. However, several thousand fatigue cycles were usually required to initiate and propagate these matrix cracks. It is anticipated that future hypersonic vehicles, particularly the first generation, will have a substantially shorter design life compared to conventional commercial and supersonic military aircraft. Therefore, the usefulness of this material system must be judged in terms of the life requirements for which it may be used, and not in terms of a design life based on millions of cycles. This material system may be sufficient for a first generation research vehicle, however, the development of better fatigue resistant materials of this type are required for an operational vehicle with longer life.

Conclusions

In this study, damage initiation and progression were investigated in $[0/90]_s$ SCS-6/Ti-15-3 laminates containing center holes. The effects of fatigue damage on the post-fatigue residual strength was determined. An effective strain parameter was used to predict the stress levels and the number of cycles to matrix crack initiation and compared to experiments. Fatigue damage progression was monitored and recorded using optical techniques and replicas (surface and edge). In general, fatigue damage consisted of fiber-matrix debonding in the 90° plies and matrix cracking from debonded surfaces. In addition, matrix cracks were observed on the surface which were bridged by the 0° fibers. As these matrix cracks progressed around the 0° fibers, fiber-matrix debonding was assumed. The stress level for matrix crack initiation and the fatigue stress limit (stress causing specimen fracture) were approximately 15% and 50% of the static notched strength, respectively. The damage developed during fatigue loading significantly reduced the composite longitudinal modulus and the static notched strength. Both the modulus and strength were reduced by 38% due to the fatigue damage. A three dimensional elastic-plastic finite element analysis was used to accurately predict the static and post-fatigue residual strengths based on the axial stress in the 0° fiber next to the hole. Both predictions were within 8% of the experimental values.

Acknowledgements

The first author gratefully acknowledges the support extended by the National Research Council, Washington, D.C., through their Associateship Program.

References

[1] Bakuckas, J. G. Jr., Awerbuch, J., Tan, T. M., and Lau, A. C. W., "Evolution of Notch-Tip Damage in Metal Matrix Composites During Static Loading," Presented at *23rd National Symposium on Fracture Mechanics,* American Society for Testing and Materials, College Station, Texas, June 11-13, 1991.

[2] Kantzos, P. and Telesman, J., "Fatigue Crack Growth Study of SCS6/Ti-15-3 Composite," *Int. J. Fatigue,* Vol 12, No. 5, September 1990, pp. 409-415.

[3] Hillberry, B. M. and Johnson, W. S., "Matrix Fatigue Crack Development in a Notched Continuous Fiber SCS-6/Ti-15-3 Composite," *Symposium on Microcracking Induced Damage in Composites,* ASME Winter Annual Meeting, Dallas, Texas, November 26-28, 1990, pp. 121-127.

[4] Johnson, W. S., "Fatigue Testing and Damage Development in Continuous Fiber Reinforced Metal Matrix Composite," *Metal Matrix Composites: Testing, Analysis, and Failure Modes, ASTM STP 1032,* W. S. Johnson, Ed., American Society for Testing and Materials, 1989, pp. 194-221.

[5] Naik, R. A., and Johnson, W. S., "Observations of Fatigue Crack Initiation and Damage Growth in Notched Titanium Matrix Composites," *Third Symposium on Composite Materials: Fatigue and Fracture, ASTM STP 1110,* T. K. O'Brien, Ed., American Society for Testing and Materials, 1991, pp. 753-771.

[6] Hillberry, B. M. and Johnson, W. S., "A Prediction of Matrix Fatigue Crack Initiation in Notched SCS-6/Ti-15-3 Metal Matrix Composites," *NASA Technical Memorandum 104141,* October 1991.

[7] Smith, K. N., Watson, R., and Topper, T. H., "A Stress-Strain Function for the Fatigue of Metals", *J. Materials, JMLSA,* Vol. 5, No. 4, 1970, pp. 767-778.

[8] Johnson, W. S., Lubowinski, S. J., and Highsmith, A. L., "Mechanical Characterization of Unnotched SCS_6/Ti-15-3 Metal Matrix Composites at Room Temperature," *Thermal and Mechanical Behavior of Metal Matrix and Ceramic Matrix Composites, ASTM STP 1080,* J. M. Kennedy, H. H. Moeller, and W. S. Johnson, Eds., American Society for Testing and Materials, 1990, pp. 193-218.

[9] Simonds, R. A., "Residual Strength of Five Boron/Aluminum Laminates with Crack-Like Notches After Fatigue Loading," *NASA Contractor Report 3815,* 1985.

[10] Jen, M. H. R., and Hsu, J. M., "Residual Strength in Notched Composite Materials," *Int. J. Fatigue,* Vol. 12, No. 4, 1990, pp. 267-274.

[11] Johnson, W. S., "Fatigue of Continuous Fiber Reinforced Titanium Metal Matrix Composites," *Mechanical Fatigue of Advanced Materials,* Ritchie, Cox and Dauskardt, Eds., MCEP Publishers, 1991.

[12] Naik, R. A., Johnson, W. S., and Dicus, D. L., "Micromechanical Thermal Analysis of Interphase Region in a Titanium Aluminide MMC," *Proceedings from Titanium Aluminide Composite Workshop,* Harry Gray Conference Center, Orlando, May 16-18, 1990, pp. 563-575. (WL-TR-91-4020, Feb. 1991)

[13] Bahei-El-Din, Y. A., and Dvorak, G. J., "Plasticity Analysis of Laminated Composite Plates," *J. Appl. Mech.*, Vol. 49, No. 4, December 1982, pp. 740-746.

[14] Bigelow, C. A., and Bahei-El-Din, Y. A., "Plastic and Failure Analysis of Composites (PAFAC). LAR-13183, COSMIC, University of Georgia, 1983.

[15] Bigelow, C. A., and Johnson, W. S., "Effect of Fiber-Matrix Debonding on Notched Strength of Titanium Metal Matrix Composites," *NASA Technical Memorandum 104131,* August 1991.

[16] Crews, J. H. Jr., "A Survey of Strength Analysis Methods for Laminates with Holes," Special Issue on Fracture Mechanics of the J. of the Aeronautical Society of India, Vol. 36, No. 4, Nov. 1984, pp. 287-303.

[17] Lekhnitskii, S. G., *Theory of Elasticity of an Anisotropic Body,* Holden-Day, San Francisco, 1963.

[18] Heywood, R. B., *Designing by Photoelasticity,* Chapman and Hall, Ltd., London (1952).

[19] Hong, C. S. and Crews, J. H., "Stress-Concentration Factors for Finite Orthotropic Laminates with a Circular Hole and Uniaxial Loading," *NASA Technical Paper-1469,* 1979.

Appendix

An orthotropic stress concentration factor K_t for a finite width specimen can be determined from the following expression [16]:

$$K_t = \alpha K_t^{\infty} \tag{A1}$$

where α and K_t^{∞} are the finite width correction factor and the stress concentration factor for an infinite orthotropic continuum, respectively. The stress concentration factor for an infinite orthotropic continuum containing a circular hole is [17]:

$$K_t^{\infty} = 1 + \sqrt{\frac{E_L}{G_{LT}} - 2\nu_{LT} + 2\sqrt{\frac{E_L}{E_T}}} \tag{A2}$$

where E_L, E_T, ν_{LT} and G_{LT} are the longitudinal modulus, transverse modulus, Poisson's ratio, and shear modulus, respectively, of the laminate as given in Table 2. The finite width correction factor for an isotropic material containing a circular hole is [18]:

$$\alpha = \frac{2 + [1 - d/W]^3}{[3(1 - d/W)]} \tag{A3}$$

where d/W is the hole diameter to specimen width ratio. It was reported in [19] that for $d/W \leq 0.33$, the isotropic finite width correction factor was within 5% of the orthotropic value for a range of orthotropic material properties which includes the SCS-6/Ti-15-3 $[0/90]_s$ laminate ($v_f = 0.355$). Thus, the isotropic finite width correction factor was used in this study. For the specimens tested in this study, $K_t = 3.72$.

Table 1. Loading History

Specimen Number	Applied Stress S_{max} (MPa)	Number of Cycles	Damage State
1	93	250,000-300,000	Initiation
	200	200,000	Progression
	265	56,169 [a]	Progression
2	80	300,000	No initiation
	150	300,000	Initiation and progression
	265	300,000	Progression
	308	1710 [a]	Progression
3	265	1,000,000	Initiation and progression
4	250	200,000	Initiation and progression

[a] catastrophic fracture occurred

Table 2. Constituent and laminate material properties of $[0/90]_s$ SCS-6/Ti-15-3, $v_f = 0.355$

Matrix [a]:	Modulus,	E_m	=	92.39 GPa
	Poisson's Ratio,	ν_m	=	0.351
	Thermal Coefficient of Expansion,	α_m	=	9.72×10^{-6} mm/mm/°C
Fiber:	Modulus [a],	E_f	=	400.00 GPa
	Poisson's Ratio [a],	ν_f	=	0.25
	Thermal Coefficient of Expansion [a],	α_f	=	4.86×10^{-6} mm/mm/°C
	Strength [b],	σ_f^{ult}	=	4400 MPa
Composite :				
	Longitudinal Modulus [c],	E_L	=	168.43 GPa
	Transverse Modulus [c],	E_T	=	168.43 GPa
	Poisson's Ratio [c],	ν_{LT}	=	0.252
	Shear Modulus [c],	G_{LT}	=	47.44 GPa
	Unnotched Strength [d],	S_{ult}^o	=	1084 MPa
	Notched Strength [d],	S_{ult}	=	525 MPa

a values taken from [8]

b strain to failure in unnotched coupon multiplied by fiber modulus

c values predicted in this study using AGLPLY [13]

d values measured in this study for one specimen

Table 3. Observed and predicted cycles to matrix crack initiation in $[0/90]_s$ SCS-6/Ti-15-3 laminates containing center hole, $v_f = 0.355$.

Applied Stress S_{max} (MPa)	Observed cycles to initiation (x1000)	Predicted cycles to initiation (x1000)
80	300 [a]	Run-out
93	250 - 300 [b]	Run-out
150	50	65
250	10	15
265	10	12

[a] test terminated

[b] initiation occurred between 250,000 and 300,000 cycles.

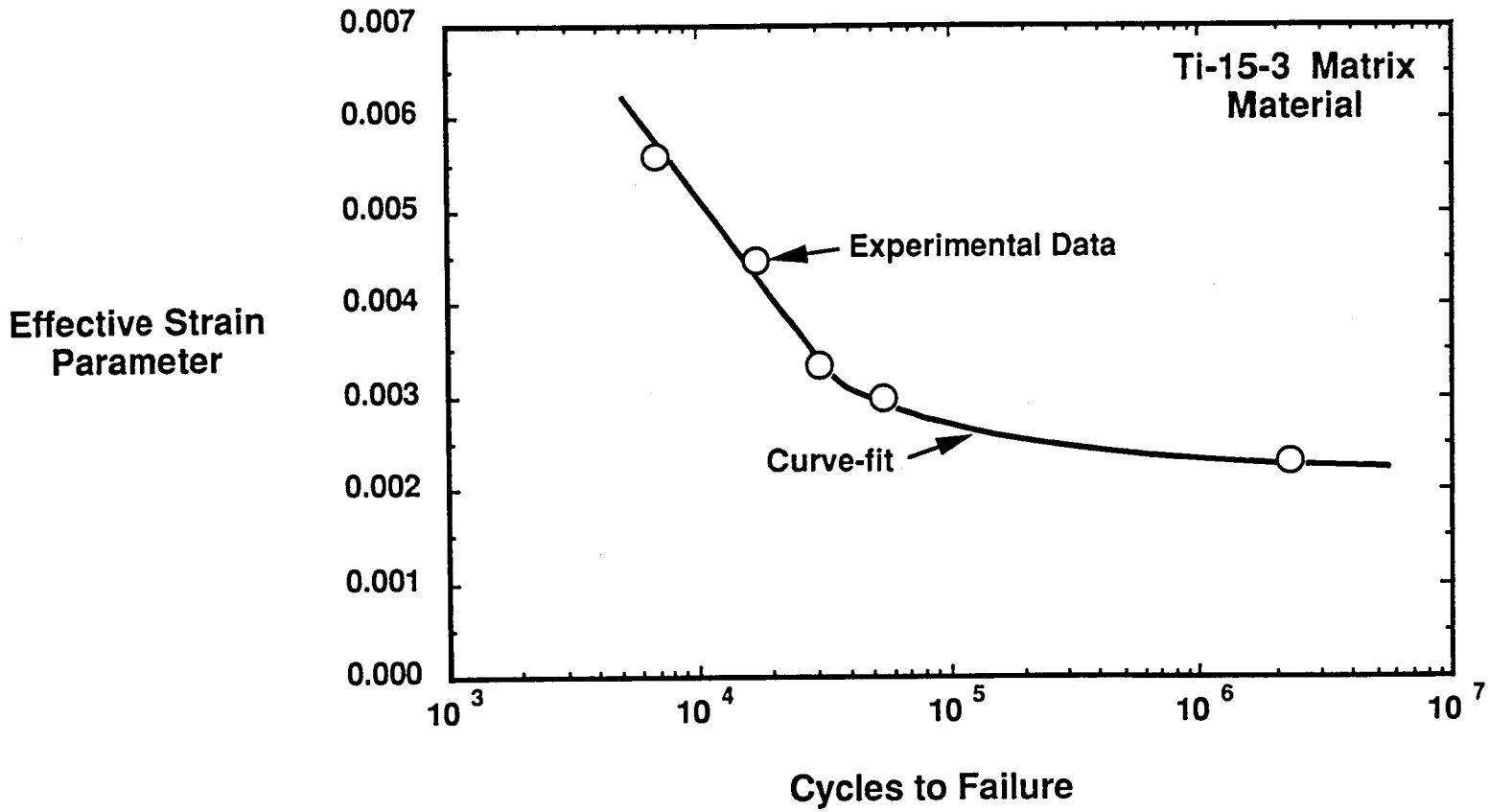

Figure 1. Modified effective strain parameter as a function of the number of cycles to failure for as-received Ti-15-3 matrix material [6].

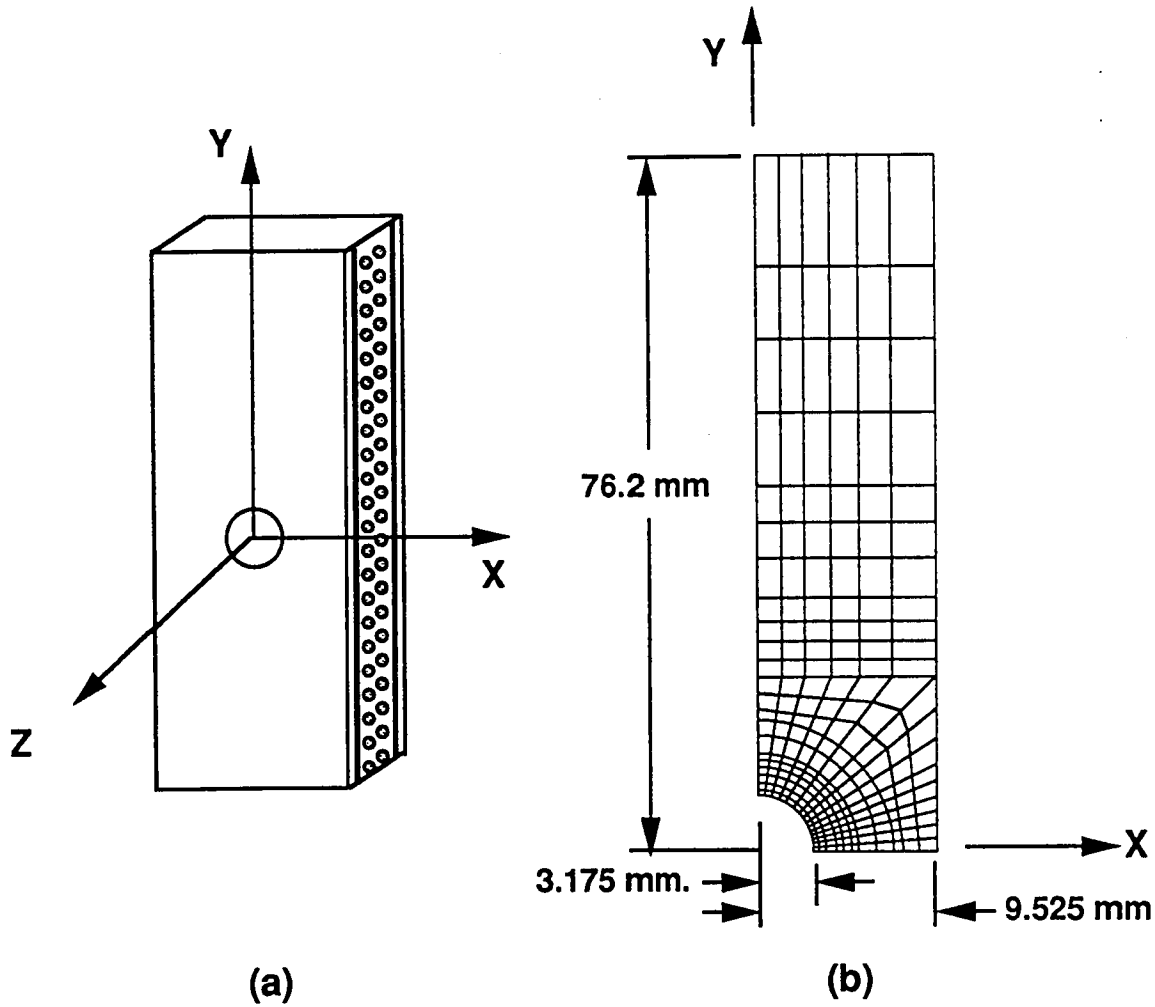

Figure 2. Specimen configuration and finite element representation for the $[0/90]_s$ SCS-6-Ti-15-3 center hole, $v_f = 0.355$; (a) center hole specimen; (b) plan view of finite element mesh.

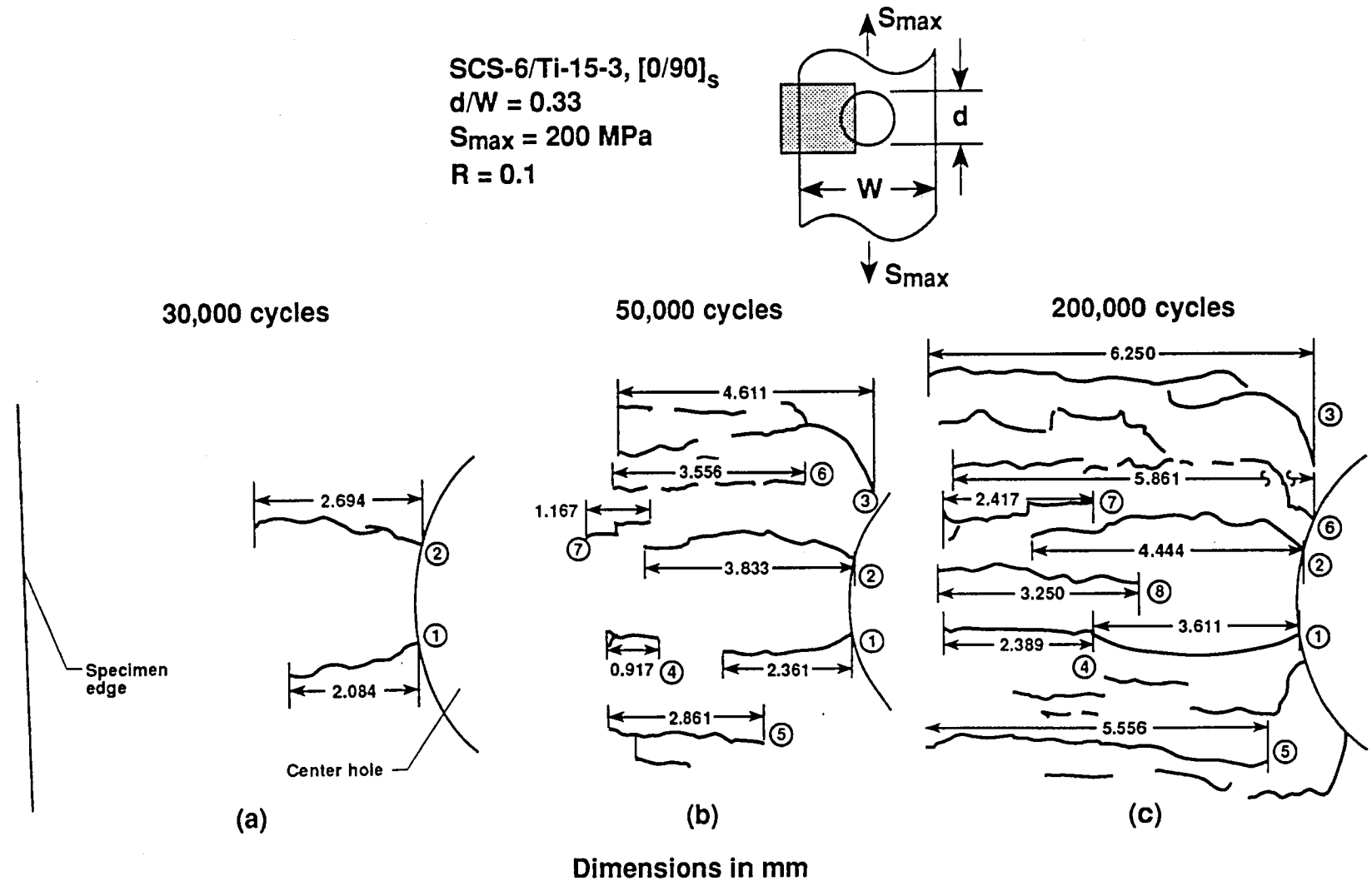

Figure 3. Development of matrix cracking in a $[0/90]_s$ SCS-6/Ti-15-3 laminate containing a center hole, v_f = 0.355; (a) initiation of cracks; (b) development of secondary cracks; (c) saturation of matrix cracks. Schematics are not to scale.

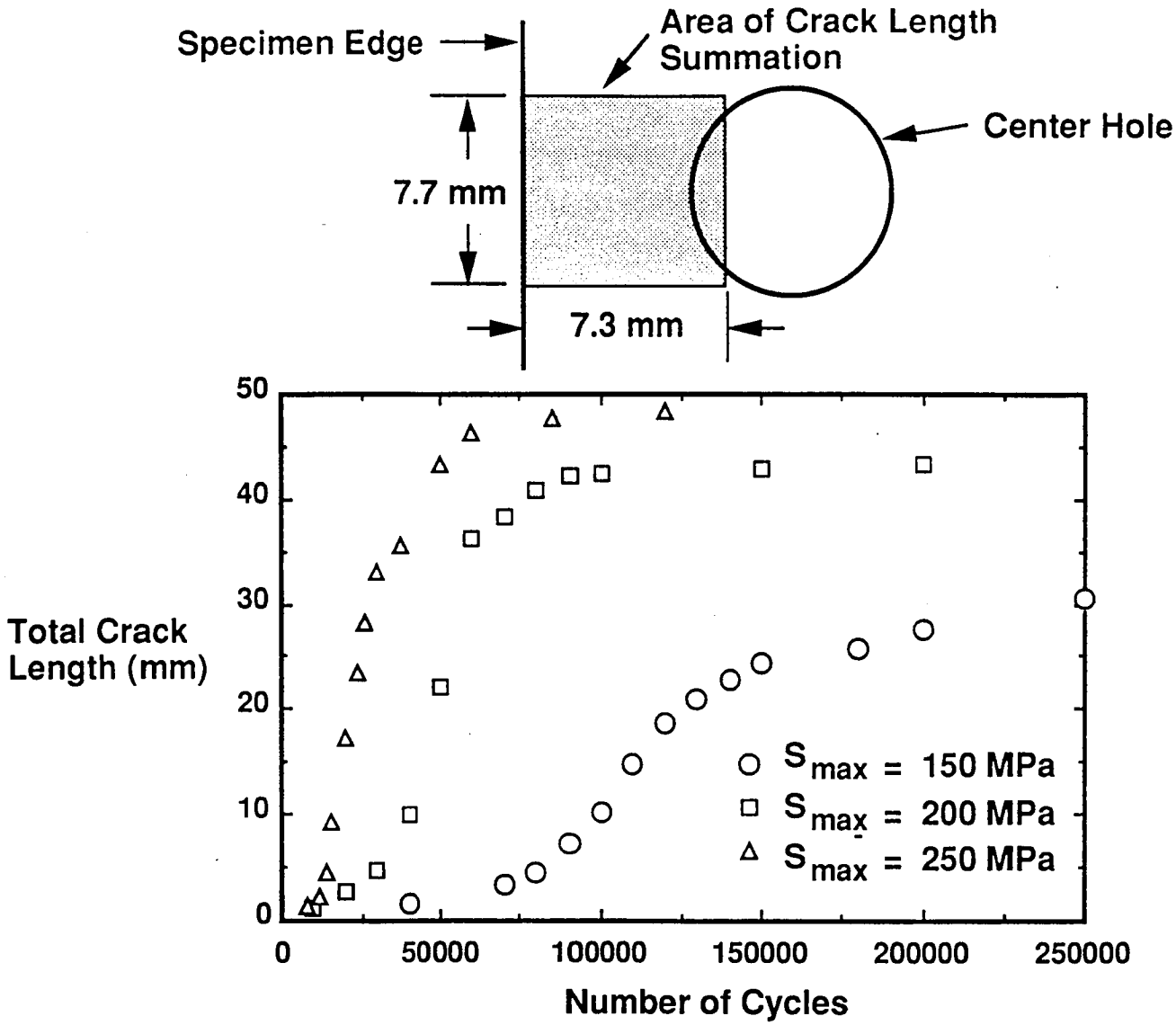

Figure 4. Effect of stress level on the total crack length in $[0/90]_s$ SCS-6/Ti-15-3 specimens containing a center hole, $v_f = 0.355$. For each stress level, the total crack length approaches a constant value corresponding to matrix crack saturation.

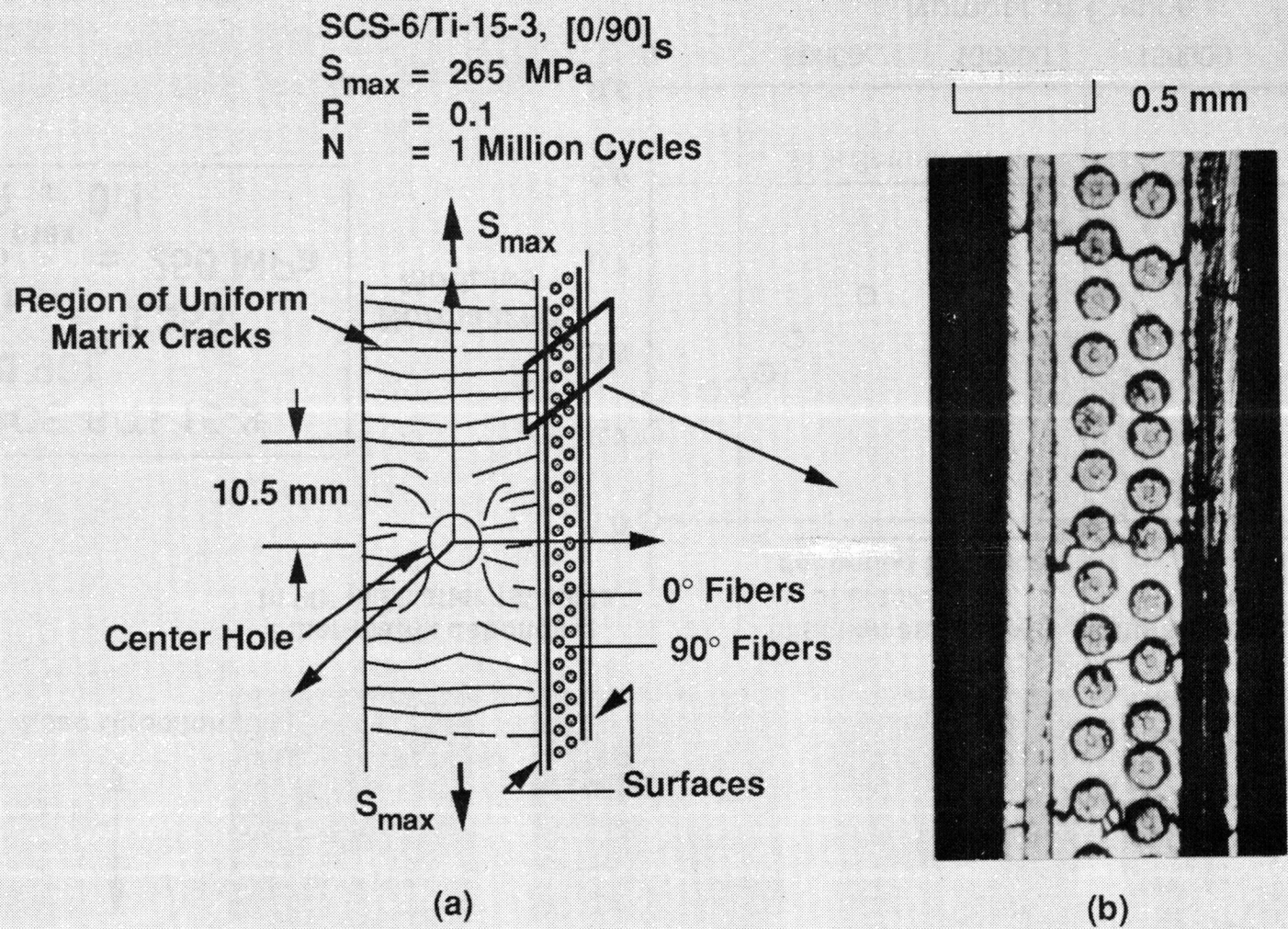

Figure 5. Matrix crack pattern in $[0/90]_s$ SCS-6/Ti-15-3 laminate after 1,000,000 cycles at S_{max} = 265 MPa, v_f = 0.355; (a) location of uniform matrix crack pattern; (b) photograph of specimen edge in region of uniform crack pattern showing through-the-thickness matrix cracks and the crack spacing.

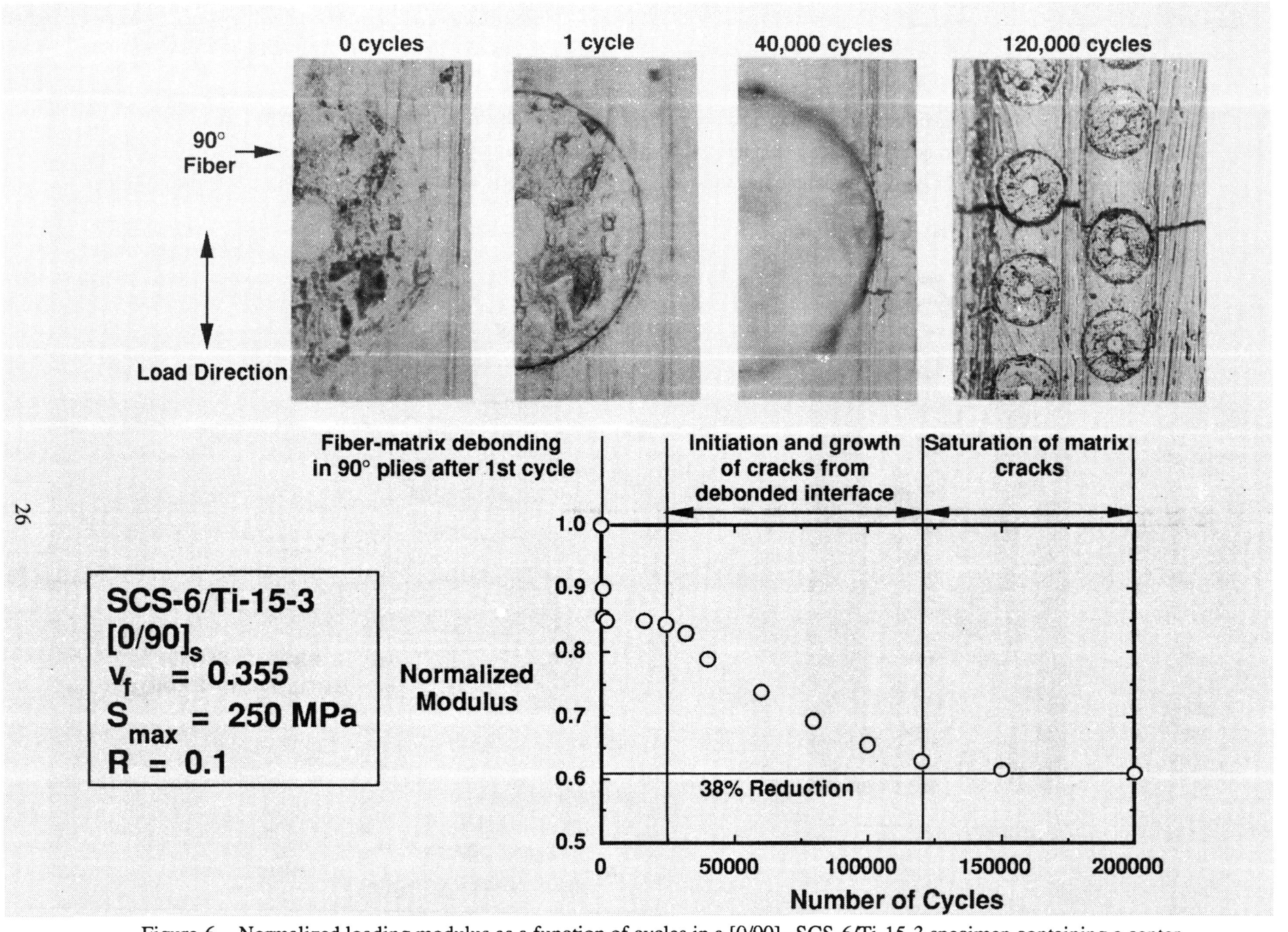

Figure 6. Normalized loading modulus as a function of cycles in a $[0/90]_s$ SCS-6/Ti-15-3 specimen containing a center hole subjected to S_{max} = 250 MPa for 200,000 cycles, v_f = 0.355. Also shown are edge replicas taken in the gage section illustrating the initiation and progression of through-the-thickness cracks. E_L = 168.43 GPa

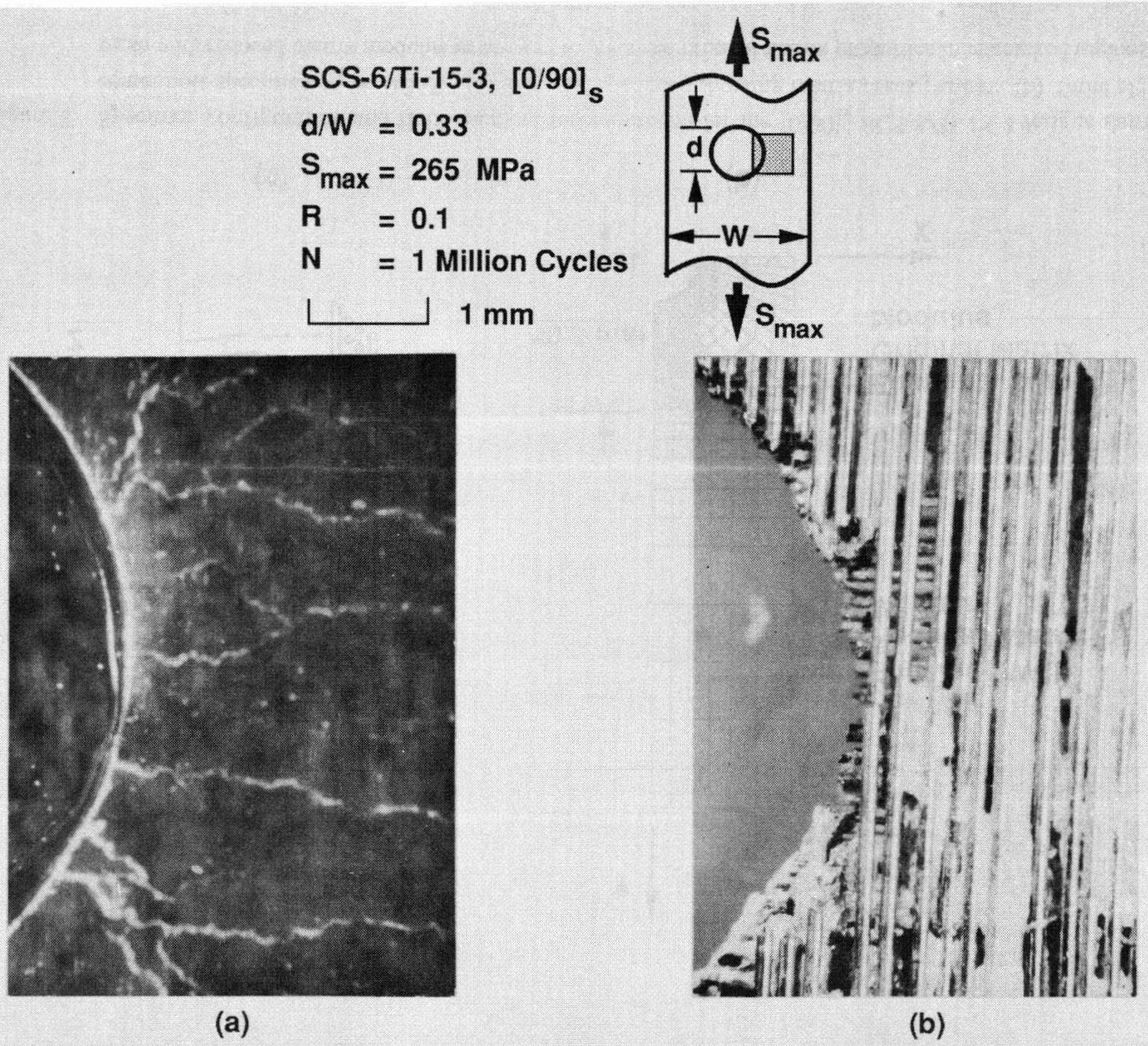

Figure 7. Photographs of the damage state developed after 1,000,000 cycles at S_{max} = 265 MPa in a $[0/90]_s$ SCS-6/Ti-15-3 laminate containing a center hole, v_f = 0.355; (a) surface replica; (b) acid etching revealing intact outer 0° fibers.

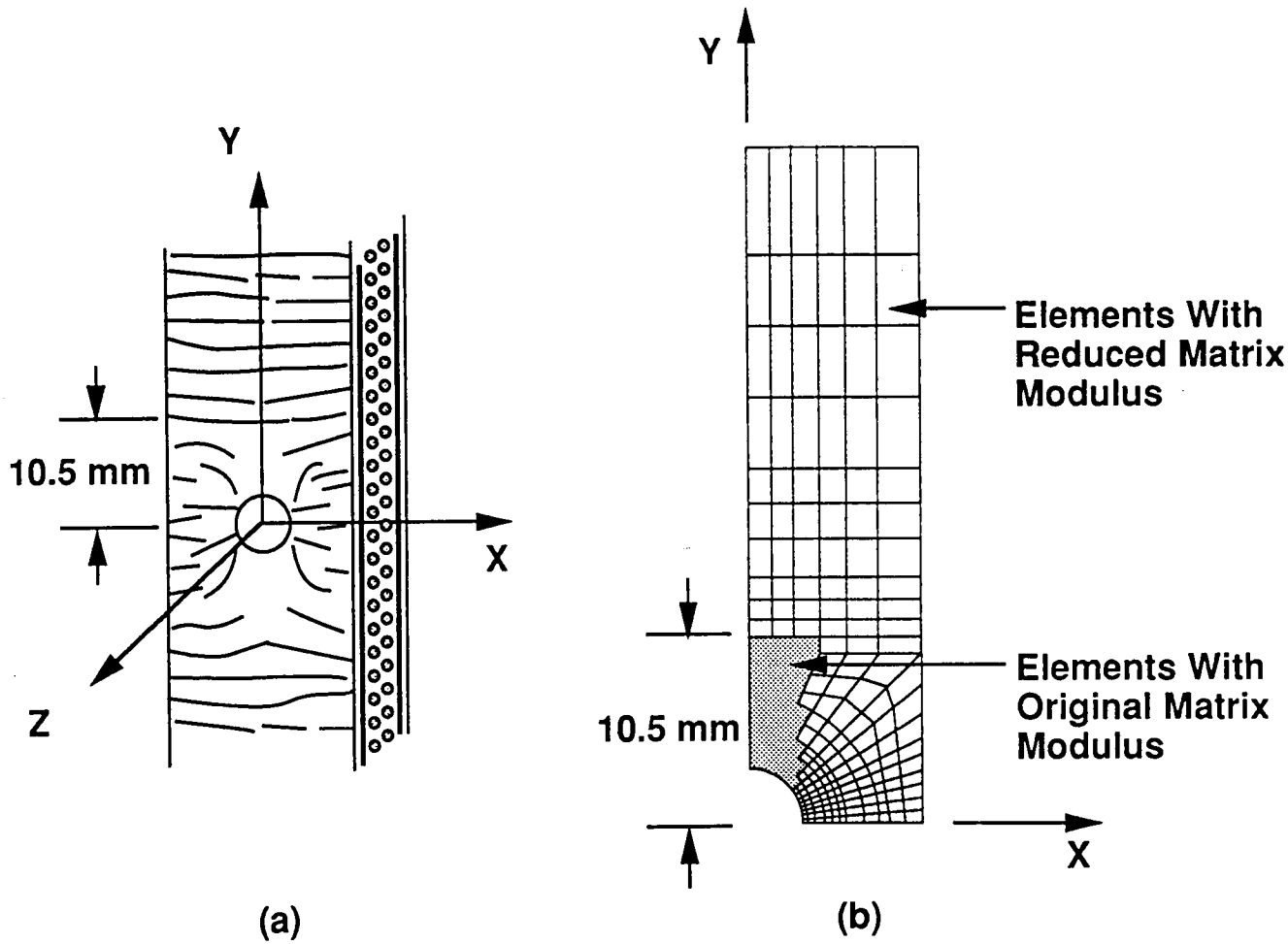

Figure 8. Specimen configuration and finite element representation for the $[0/90]_s$ SCS-6/Ti-15-3 fatigue damaged center hole specimen, $v_f = 0.355$; (a) damaged specimen showing matrix crack pattern; (b) finite element mesh with reduced matrix modulus in cracked regions and original matrix properties in uncracked regions.

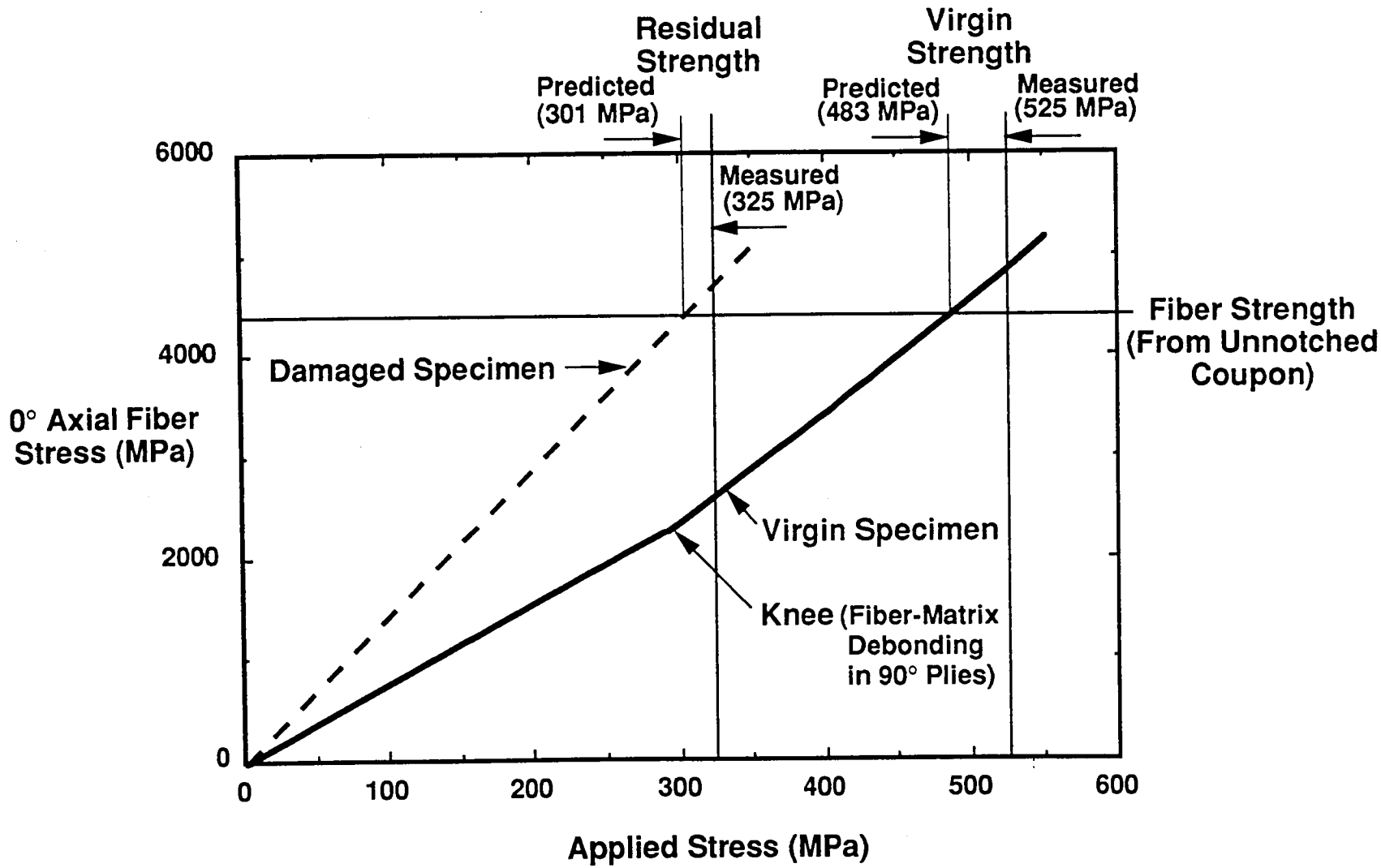

Figure 9. Axial stress in 0° fiber next to the hole as a function of applied stress for the virgin and post-fatigue conditions in $[0/90]_s$ SCS-6/Ti-15-3 laminate, $v_f = 0.355$. Applied stress at which the 0° fiber stress reaches the fiber strength corresponds to the notched strength for both conditions.

REPORT DOCUMENTATION PAGE

Form Approved
OMB No. 0704-0188

1. AGENCY USE ONLY (Leave blank)	2. REPORT DATE	3. REPORT TYPE AND DATES COVERED
	January 1992	Technical Memorandum

4. TITLE AND SUBTITLE

Fatigue Damage in Cross-Ply Titanium Metal Matrix Composites Containing Center Holes

5. FUNDING NUMBERS

506-43-71-01

6. AUTHOR(S)

J. G. Bakuckas, Jr.; W. S. Johnson; and C. A. Bigelow

7. PERFORMING ORGANIZATION NAME(S) AND ADDRESS(ES)

NASA Langley Research Center
Hampton, VA 23665-5225

8. PERFORMING ORGANIZATION REPORT NUMBER

9. SPONSORING/MONITORING AGENCY NAME(S) AND ADDRESS(ES)

National Aeronautics and Space Administration
Washington, D.C. 20546

10. SPONSORING/MONITORING AGENCY REPORT NUMBER

NASA TM-104197

11. SUPPLEMENTARY NOTES

Bakuckas: NRC, Langley Research Center, Hampton, VA; Johnson and Bigelow, NASA Langley Research Center, Hampton, VA 2665-5225

12a. DISTRIBUTION/AVAILABILITY STATEMENT

Unclassified - Unlimited

Subject Category - 24

12b. DISTRIBUTION CODE

13. ABSTRACT (Maximum 200 words)

The development of fatigue damage in $[0/90]_s$ SCS-6/TI-15-3 laminates containing center holes was investigated. Stress levels required for crack initiation in the matrix were predicted using an effective strain parameter and compared to experimental results. Damage progression was monitored at various stages of fatigue loading. In general, a saturated state of damage consisting of matrix cracks and fiber-matrix debonding was obtained which reduced the composite modulus. Matrix cracks were bridged by the 0° fibers. The fatigue limit (stress causing catastrophic fracture of the laminates) was also determined. The static and post-fatigue residual strengths were accurately predicted using a three dimensional elastic-plastic finite element analysis. The matrix damage that occurred during fatigue loading significantly reduced the notched strength.

14. SUBJECT TERMS

Crack initiation prediction; Fiber-matrix debonding; Matrix cracking;Fiber bridging; Modulus reduction

15. NUMBER OF PAGES
30

16. PRICE CODE
A03

17. SECURITY CLASSIFICATION OF REPORT	18. SECURITY CLASSIFICATION OF THIS PAGE	19. SECURITY CLASSIFICATION OF ABSTRACT	20. LIMITATION OF ABSTRACT
Unclassified	Unclassified		